

HIGH-ENERGY LHC DESIGN*

D. Amorim, S.A. Antipov, S. Arsenyev, M. Benedikt, R. Bruce, M. Crouch, S. Fartoukh, M. Giovannozzi, B. Goddard, M. Hofer, R. Kersevan, V. Mertens, Y. Muttoni, J. Osborne, V. Parma, V. Raginel, S. Redaelli, T. Risselada, I. Rühl, B. Salvant, D. Schoerling, E. Shaposhnikova, L. Tavian, E. Todesco, R. Tomas, D. Tommasini, F. Valchkova-Georgieva, V. Venturi, D. Wollmann, F. Zimmermann[†], CERN, Geneva, Switzerland; A. Apyan, ANSL, Yerevan, Armenia; G. Guillermo Cantón, CINVESTAV Mérida, Mexico; F. Burkart, DESY, Hamburg, Germany; J. Barranco, L. Mether, T. Pieloni, L. Rivkin, C. Tambasco, EPFL, Lausanne, Switzerland; J.L. Abelleira, E. Cruz-Alaniz, P. Martinez Mirave, A. Seryi, L. van Riesen-Haupt, JAI Oxford, U.K.; K. Ohmi, K. Oide, D. Zhou, KEK, Ibaraki, Japan; Y. Cai, Y. Nosochkov, SLAC, Menlo Park, U.S.A.

Abstract

In the frame of the FCC study we are designing a 27 TeV hadron collider in the LHC tunnel, called the High Energy LHC (HE-LHC).

PARAMETER CHOICES

The HE-LHC shall provide proton-proton collisions at an energy of about 27 TeV in the centre of mass. Its integrated luminosity should exceed 10 ab^{-1} over 20 years of operation. The HE-LHC will employ FCC dipole magnets with a field of 16 T [1, 2]. The expected photon flux and synchrotron radiation power are 5–20 times higher than for the LHC. The FCC-hh beam screen design [3] offers an adequate solution, with high pumping capacity, low impedance, and a good Carnot efficiency. The HE-LHC also incorporates novel elements from the HL-LHC [4, 5], such as crab cavities and low-impedance collimators.

The HE-LHC could accommodate two high-luminosity interaction-points (IPs) 1 and 5, at the locations of the present ATLAS and CMS experiments. IPs 2 and 8 might host secondary experiments (or a lepton-hadron collision point) combined with injection, as for the LHC.

Following the LHC injector upgrade (LIU) [6], in 2020, a brighter proton beam will be available. Injection into the HE-LHC could be accomplished from the present SPS at 450 GeV, from a new fast ramping single-layer coil superconducting (SC) synchrotron in the SPS tunnel at 900 GeV [7], or from a double-layer coil SC synchrotron at 1.3 TeV [7, 8].

The HE-LHC itself must fit into the existing LHC tunnel with a typical diameter of 3.8 m. Therefore, the outer diameter of its dipole magnets is restricted to 1.2 m, while half sector cooling reduces the size of the cryogenics lines. Overall, the HE-LHC will need up to eight new cryoplants, each with 1.5 times the capacity of one of the existing eight LHC plants, and additional plants at 1.8 K. Two new underground cubes (10 m sides) are required at IPs 3 and 7.

The HE-LHC baseline design parameters are summarized in Table 1, which also presents a comparison with the corresponding values for LHC, HL-LHC and FCC-hh [9].

* This work was supported by the European Commission under the HORIZON 2020 projects EuroCirCol, grant agreement no. 654305; EASITrain no. 764879; and ARIES no. 730871.

[†] frank.zimmermann@cern.ch

LUMINOSITY PERFORMANCE

Radiation damping is significant. The longitudinal emittance needs to be kept constant during the physics store, through longitudinal noise excitation, in order to maintain longitudinal Landau damping [10]. At the same time, the transverse emittance shrinks due to radiation damping, while the proton intensity decreases as the result of the high luminosity. The initial proton burn-off time is

$$\tau_{\text{bo}} = \frac{N_b n_b}{L_0 \sigma_{\text{tot}} n_{\text{IP}}}, \quad (1)$$

where N_b denotes the bunch population, L_0 the initial luminosity, σ_{tot} the total proton-proton cross section, n_b the number of bunches per beam, and n_{IP} ($= 2$) the number of high-luminosity interaction points (IPs). The HE-LHC proton burn-off time is comparable to the transverse emittance damping time τ , yielding a natural luminosity leveling, while the beam-beam tune shift decreases during the store.

Following [9, 11], the integrated luminosity per interaction point (IP) at time t during the fill is

$$\int_0^t L(t) dt = \frac{f_{\text{rev}} N_{b,0}^2 n_b}{4\pi \varepsilon_0 \beta_{x,y}^*} \frac{\tau}{B} \left(1 - \frac{1}{1 - B + B \exp(t/\tau)} \right), \quad (2)$$

from which the optimum fill length can be determined, with

$$B \equiv \frac{\sigma_{\text{tot}} n_{\text{IP}} f_{\text{rev}} N_{b,0} \tau}{4\pi \beta_{x,y}^* \varepsilon_0}, \quad (3)$$

where ε_0 denotes the initial rms emittance, $N_{b,0}$ the initial bunch population, and f_{rev} the revolution frequency.

Figure 1 shows the time evolution of key parameters over 24 hours at 100% availability. The typical optimum fill length of HE-LHC is about 3 hours. The turnaround time determines the integrated luminosity, as illustrated in Fig. 2.

OPTICS

The choice of the HE-LHC arc optics will be a compromise between maximizing the energy reach (favouring fewer and longer cells) and allowing injection from the existing SPS (calling for a larger number of shorter cells). Exploring the parameter space, we are considering two alternative arc optics: The first one, denoted “18 × 90”, features 18 FODO

Table 1: Key parameters of HE-LHC compared with FCC-hh, HL-LHC [12] and LHC [13], for operation with proton beams. All values, except for the injection energy, refer to collision energy. HE-LHC entries shown in parentheses refer to a larger crossing angle; LHC entries in parentheses to the HL-LHC. The bunch spacing is 25 ns for all colliders

parameter	unit	FCC-hh	HE-LHC	(HL-)LHC
centre-of-mass energy	TeV	100	27	14
injection energy	TeV	3.3	0.45/0.9/1.3	0.45
arc dipole field	T	16	16	8.33
circumference	km	97.8	26.7	26.7
beam current	A	0.5	1.12	(1.12) 0.58
bunch population N_b	10^{11}	1.0	2.2	(2.2) 1.15
longitudinal emittance ($\sim 4\pi\sigma_z\sigma_E$)	eVs	5	4.2	2.5
norm. transv. rms emittance $\gamma\varepsilon$	μm	2.2	2.5	(2.5) 3.75
IP beta function $\beta_{x,y}^*$	m	1.1	0.3	0.25
peak luminosity per IP	$10^{34} \text{ cm}^{-2}\text{s}^{-1}$	5	30	28
peak no. of events / crossing	—	170	1000	800
SR power / beam	kW	2400	100	(7.3) 3.6
transv. emittance damping time τ	h	1.1	3.6	25.8
initial proton burn-off time τ_{bo}	h	17	3.4	2.5
luminosity per year (160 days)	fb^{-1}	≥ 250	≥ 1000	730
				(250) 55

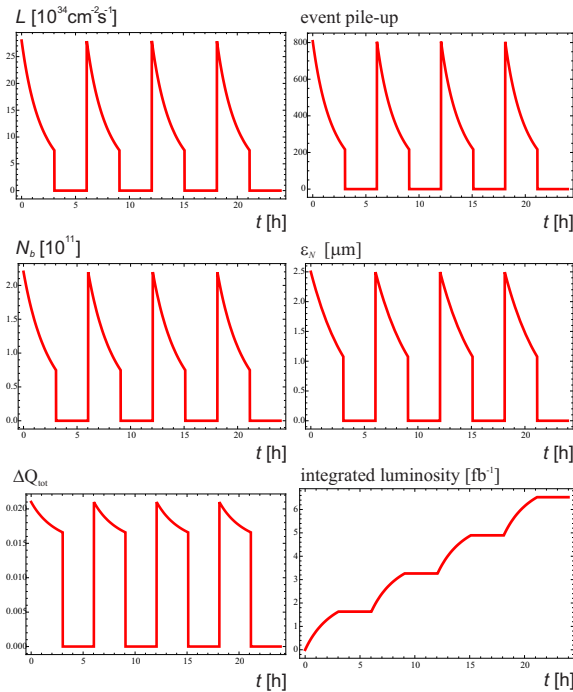


Figure 1: Instantaneous luminosity, pile-up, bunch population, normalized transverse emittance, total beam-beam tune shift, and integrated luminosity as a function of time during 24 hours, for the HE-LHC at 100% machine availability.

cells per arc and 90 degree phase advance per cell. The second optics, referred to as “ 23×90 ”, consists of 23 cells per arc, similar to the present LHC optics. Both optics follow the footprints of LEP and LHC, to within a few centimetres. Table 2 compiles key parameters. At 450 GeV, for the 23×90 optics the minimum physical aperture in every regular arc

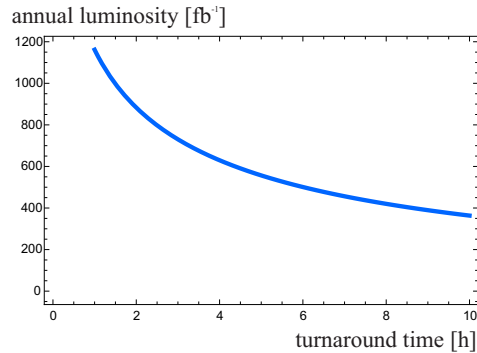


Figure 2: Average annual luminosity versus average turnaround time (nominal value 3 hours) for the HE-LHC, assuming 160 calendar days scheduled for physics operation per year and 70% machine availability.

cell is about 9.5σ , for the 18×90 optics only 7.2σ [14], using the parameters of [15] and a mechanical tolerance of 1 mm. These numbers are smaller than the minimum aperture of 12.6σ for the HL-LHC [16]. They might become acceptable with a stricter control of injection oscillations, adequate machine protection measures, and tighter primary collimator settings. For example, above the primary collimators set at 5σ another 4.5σ (23×90) or 2.2σ (18×90) [present LHC: $\sim 9 \sigma$] would be available for preserving the collimator hierarchy between primary, secondary, and dump-protection collimators, and the arc aperture.

The calculated multipole field errors for the Nb_3Sn magnets of the HE-LHC are shown in Table 3, which assumes a SC wire filament size of $20 \mu\text{m}$. For the 18×90 optics, including b_3 , b_4 and b_5 correctors, the simulated dynamic aperture (10^5 turns, 60 seeds, $\Delta p/p = 0.075\%$) is 4.8σ at 1.3 TeV, and significantly less at lower energies. For the

Content from this work may be used under the terms of the CC BY 3.0 licence (© 2018). Any distribution of this work must maintain attribution to the author(s), title of the work, publisher, and DOI.

This is a preprint — the final version is published with IOP

Table 2: Arc Optics Parameters for LHC (scaled to a Beam Energy of 13.5 TeV) and the two HE-LHC Optics Desins

parameter	unit	23 × 90	18 × 90
cell length	m	106.9	137.2
quadrupole length	m	3.5	2.8
max., min. beta	m	177, 32	230, 40
max., min. dispersion	m	2.2, 1.1	3.6, 1.8
dipole field for 13.5 TeV	T	16.59	15.83
c.m. energy for 16 T dip.	TeV	26.01	27.28

23 × 90 optics, it is 2.8 σ at 450 GeV, 1.0 σ (!) at 900 GeV, and 11.9 σ at 1.3 TeV [14]. At present only this last case looks viable. However, adding artificial pinning centers (APC) and either magnetic iron shims [17] or HTS persistent-current shims [18] could further reduce the field errors [19]. Improved correction schemes may also help.

More details on the arc optics can be found in Ref. [20]. An integrated overall HE-LHC optics exists at injection and collision energies [14]. It includes the experimental insertions [21, 22], betatron collimation straight [23], injection and extraction straights [24], and rf straight [25].

Table 3: Systematic, uncertainty and random normal sextupole component b_3 in the main arc dipoles, in units of 10^{-4} at a reference radius of 16.7 mm, for three different injection energies, considering a wire with 20 μm filament size and $\pm 5\%$ critical current variation [16]

energy	syst.	uncertainty	random
450 GeV	-35	10	10
900 GeV	-55	4	4
1.3 TeV	-40	3	3

COLLECTIVE EFFECTS

Beam-beam effects in HE-LHC are discussed in [26]. Extrapolating from LHC studies and HL-LHC simulations [27], a 180 μrad half crossing angle will ensure adequate dynamic aperture. The crossing angle could also be reduced, e.g. to 130 μrad , by adding a beam-beam compensation scheme.

The beam screen and the collimators are the major sources of HE-LHC impedance [28, 29]. The beam-screen impedance is increased compared with the present LHC due to the smaller half aperture (12 versus ~ 18 mm in the vertical plane) and higher beam-screen temperature (50 K for HE-LHC versus 5–20 K for LHC). The collimators are a major contributor to the transverse impedance since they are operated with small gaps. It is assumed that the physical gaps of the collimators become tighter as the beam energy increases, so that the collimation system becomes the main impedance source already at 1.3 TeV. The impedance for warm beam pipes and other components can be taken from

the LHC [30]. The complete transverse impedance [31] is illustrated in Fig. 3 for two different injection energies. For comparison the HL-LHC impedance is also shown. At 450 GeV the HE-LHC impedance is about a factor 2–3 higher than the HL-LHC impedance, due to the changes in the beam screen. At 1.3 TeV the HE-LHC impedance is even larger because of the tighter collimator gaps.

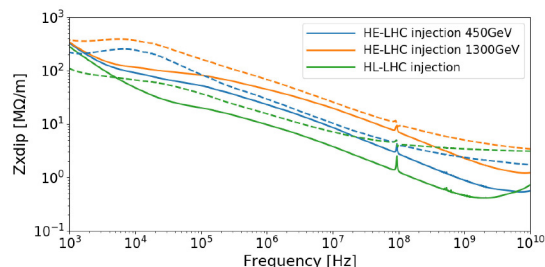


Figure 3: Real (solid curves) and imaginary part (dashed curves) of the HE-LHC transverse impedance at two different injection energies compared with the HL-LHC transverse impedance, as a function of frequency [31].

Using the impedance model, the stability limits can be explored with a Vlasov solver, such as NHT [32] or DELPHI [33]; the results of the two codes are consistent for single bunches [34]. The coupled-bunch instability modes will be cured by the transverse feedback, while single-bunch instabilities can be suppressed by Landau damping provided either through octupole magnets [26] or electron lenses [35].

Electron cloud is important at the present LHC [36] and a concern for HL-LHC. For HE-LHC, build-up simulations were performed for two different beam-screen designs [37], namely the FCC-hh type beam screen, adapted as baseline, and a scaled LHC beam screen of larger aperture [38]. At top energy, up to maximum SEY values of 1.7, or higher, the simulated electron density stays below the instability threshold [39], for both chamber options. However, the FCC beam screen gives rise to a ten times lower density, reflecting the smaller amount of photoelectron seeding. Also the heat load produced by the electron cloud is lower for the FCC beam screen. If the maximum secondary emission yield is below 1.5 the heat load from electron cloud amounts to less than 10% of the synchrotron-radiation power [37].

SUMMARY

An HE-LHC optics solution with 1.3 TeV injection and 13.5 TeV top energy is (nearly) at hand. This would require a new superconducting SPS as injector. We are also investigating an alternative optics for injection at 450 (or 900) GeV with 13 TeV top energy. Related magnet design improvements are under study (e.g., active pinning centres and shimming). Challenges for the lower injection energy include physical and dynamic aperture, machine protection and collimation. Collective effects appear under control.

The HE-LHC 16 T Nb₃Sn magnets (compact and curved), cryogenics system, and tunnel integration are not trivial.

REFERENCES

- [1] M. Benedikt and F. Zimmermann, "Towards Future Circular Colliders," *Journal Korean Physical Society* 69 (2016) 893.
- [2] M. Benedikt, "FCC: Colliders at the Energy Frontier," presented at IPAC'18, Vancouver, THYGBD1, this conference.
- [3] R. Kersevan, International Conference on High Energy Physics 2016, Chicago, U.S.A. (2016).
- [4] G. Apollinari et al., "High-Luminosity Large Hadron Collider (HL-LHC): Technical Design Report V. 0.1", CERN Yellow Report CERN-2017-007-M (2017).
- [5] L. Medina Medrano et al., "New HL-LHC Baseline and Performance at Ultimate Energy," presented at IPAC'18, Vancouver, MOPML009, this conference.
- [6] H. Damerau et al., "LHC Injectors Upgrade, Technical Design Report, Vol. I: Protons", CERN-ACC-2014-0337 (2014).
- [7] FCC Conceptual Design Report, volume 6, High Energy LHC Summary, in preparation.
- [8] F. Burkart et al., "Conceptual Design Considerations for a 1.3 TeV superconducting SPS (scSPS)," in *Proc. IPAC'17 Copenhagen* (2017).
- [9] M. Benedikt, D. Schulte, F. Zimmermann, "Optimizing Integrated Luminosity of Future Hadron Colliders," *Phys. Rev. ST Accel. Beams* 8, 101002 (2015).
- [10] F. Zimmermann, "Luminosity Limitations at Hadron Colliders," in *Proc. 18th International Conference on High-Energy Accelerators (HEACC'01)*, Tsukuba, 26–30 March, 2001; also published as CERN-SL-2001-009-AP (2001).
- [11] M. Benedikt and F. Zimmermann, "Proton Colliders at the Energy Frontier," submitted to NIM A Siegbahn issue, arXiv 1803.09723 (2018).
- [12] HiLumi LHC Technical Coordination Committee, <http://espace.cern.ch/HiLumi/TCC>, "Parameters".
- [13] O. Brüning et al., "LHC Design Report, Volume v.1: The LHC Main Ring," CERN-2004-003-V-1 (2004).
- [14] L. van Riesen-Haupt et al., "Integrated Full HE-LHC Optics and Its Performance," presented at IPAC'18, Vancouver, MOPMK002, this conference.
- [15] R. Bruce et al., "Parameters for aperture calculations at injection for HL-LHC", CERN-ACC-2016-0328 (2016).
- [16] S. Izquierdo Bermudez et al., "Multipole field errors for HE-LHC with an effective filament size of 20 μm and $\pm 5\%$ critical-current variation," private communication, to be published in the FCC Conceptual Design Report (2018).
- [17] V.V. Kashikhin, A.V. Zlobin, "Persistent Current Effect in 15-16 T Nb₃Sn Accelerator Dipoles and its Correction", in *Proc. NAPAC2016* (2016).
- [18] J. van Nugteren et al., "Persistent Current Shim Coils for Accelerator Magnets", CERN TE-MS-C Internal Note 2016-03, EDMS Nr. 1574002 (2014).
- [19] D. Schoerling, " b_2/b_3 Shimming Recipe and Prospects", HE-LHC Design Meeting no. 26, 8 March 2018, to be published in the FCC Conceptual Design Report (2018).
- [20] Y. Nosochkov et al., "Optimized Arc Optics for the HE-LHC," presented at IPAC'18, Vancouver, MOPMF067.
- [21] L. van Riesen-Haupt et al., "Experimental Interaction Region Optics for the HE-LHC," presented at IPAC'18, Vancouver, MOPMK006, this conference.
- [22] J. Abelleira et al., "HE-LHC Final Focus: Flat Beam Parameters and Energy Deposition Studies," presented at IPAC'18, Vancouver, MOPMK005, this conference.
- [23] M. Crouch et al., "A First Design of the Proton Collimation System for the HE-LHC," unpublished article (2018).
- [24] W. Bartmann et al., "Injection and Dump Systems for a 13.5 TeV Hadron Synchrotron HE-LHC," presented at IPAC'18, Vancouver, TUPAF060, this conference.
- [25] L. van Riesen-Haupt et al., "Optics for RF Acceleration Section in IR4 for the High Energy LHC," presented at IPAC'18, Vancouver, MOPMK001, this conference.
- [26] T. Pieloni et al., "The High-Energy LHC Beam-Beam Effects Studies," presented at IPAC'18, Vancouver, MOPMF069.
- [27] T. Pieloni et al., "Beam-Beam Effects Long-Range and Head-On," in *Proc. 6th Evian Workshop*, CERN-ACC-2015-376 (2015).
- [28] S. Arsenyev, "Impedance Aspects of the Beamscreen," HE-LHC Design Review, CERN, 11-12 December 2017 (2017); to be published in the FCC Conceptual Design Report (2018).
- [29] S. Arsenyev, D. Schulte, "Geometrical Impedance of Pumping Holes and Tapers in the FCC-hh Beamscreen," presented at IPAC'18, Vancouver, MOPMF030, this conference.
- [30] B. Salvant et al., "HL-LHC impedance," in preparation.
- [31] D. Amorim et al., "Impedance Model for HE-LHC," HE-LHC Design Review, CERN, 11-12 December 2017 (2017); to be published in the FCC Conceptual Design Report (2018).
- [32] A. Burov, "Nested head-tail Vlasov solver," *Phys. Rev. Accel. Beams* 17, 021007 (2014).
- [33] N. Mounet, "DELPHI: an analytic Vlasov solver for impedance-driven modes," Talk presented at HSC meeting, CERN, 09 April 2014, <https://espace.cern.ch/be-dep-workspace/abp/-HSC/Meetings/DELPHI-expanded.pdf> (2014).
- [34] S. Antipov et al., "HE-LHC Instability Growth Rates," HE-LHC Design Review, CERN, 11-12 December 2017 (2017); to be published in the FCC Conceptual Design Report (2018).
- [35] V. Shiltsev, Y. Alexahin, A. Burov, and A. Valishev, "Landau Damping of Beam Instabilities by Electron Lenses," *Phys. Rev. Lett.* 119, 134802 (2017)
- [36] L. Tavian, "Report from the task force on beam-induced heat load," presented at LHC Performance Workshop 2018, Chamonix (2018).
- [37] L. Mether, in D. Amorim et al., "Single-Beam Transverse Collective Effects for HE-LHC," ICFA Beam Dynamics Newsletter no. 72, Dec. 2017, <http://icfa-bd.kek.jp/news.html> (2017).
- [38] G. Guillermo, D. Sagan, F. Zimmermann, "Examining Mitigation Schemes for Synchrotron Radiation in High-Energy Hadron Colliders," *Phys. Rev. Accel. Beams* 21, 021001 (2018).
- [39] K. Ohmi, F. Zimmermann, and E. Perevedentsev, "Wake-field and fast head-tail instability caused by an electron cloud," *Phys. Rev. E* 65, 016502 (2001).